Computers in Biology and Medicine 104 (2019) 62–69

Contents lists available at ScienceDirect

Computers in Biology and Medicine

journal homepage: www.elsevier.com/locate/compbiomed

Exudate detection in fundus images using deeply-learnable features

Parham Khojasteh[a,*], Leandro Aparecido Passos Júnior[b], Tiago Carvalho[c], Edmar Rezende[d], Behzad Aliahmad[a], João Paulo Papa[e], Dinesh Kant Kumar[a]

[a] Royal Melbourne Institute of Technology, Biosignals Laboratory, School of Engineering, 124 La Trobe St, Melbourne, Australia
[b] Federal University of São Carlos, Department of Computing, Rod. Washington Luís, Km 235, São Carlos, 13565-905, Brazil
[c] Federal Institute of São Paulo, Department of Computing, Campinas, 13069-901, Brazil
[d] University of Campinas, Institute of Computing, Campinas, 13069-901, Brazil
[e] São Paulo State University - UNESP, Department of Computing, Av. Eng. Luiz Edmundo Carrijo Coube, 14-01, Bauru, 17033-360, Brazil

ARTICLE INFO

Keywords:
Exudate detection
Deep learning
Convolutional neural networks
Deep residual networks
Discriminative restricted Boltzmann machines
Diabetic retinopathy

ABSTRACT

Presence of exudates on a retina is an early sign of diabetic retinopathy, and automatic detection of these can improve the diagnosis of the disease. Convolutional Neural Networks (CNNs) have been used for automatic exudate detection, but with poor performance. This study has investigated different deep learning techniques to maximize the sensitivity and specificity. We have compared multiple deep learning methods, and both supervised and unsupervised classifiers for improving the performance of automatic exudate detection, i.e., CNNs, pre-trained Residual Networks (ResNet-50) and Discriminative Restricted Boltzmann Machines. The experiments were conducted on two publicly available databases: (i) DIARETDB1 and (ii) e-Ophtha. The results show that ResNet-50 with Support Vector Machines outperformed other networks with an accuracy and sensitivity of 98% and 0.99, respectively. This shows that ResNet-50 can be used for the analysis of the fundus images to detect exudates.

1. Introduction

Undiagnosed diabetic retinopathy (DR) leads to vision impairment and blindness and its early detection can significantly reduce this by 50% [1–5]. Presence of exudates in fundus images is one of the early signs of DR [6]. However, manual detection of exudates is dependent on the examiner and is time-consuming. Automatic exudate detection would make it possible to perform widespread screening of at-risk population, and for remote communities. This is a very challenging task due to factors such as uneven illumination, poor contrast and variability of size, color, texture and shape of the exudates.

A number of image processing and machine learning approaches have been proposed for exudate detection using fundus images [7–12]. In 2008, Sopharak et al. [13] used a mathematical morphology-based method to detect exudates on retinal images of non-dilated eyes, and later Sanchez et al. [14] used a statistical mixture model-based clustering for dynamic thresholding to identify the exudate pixels. García et al. [15] applied three different classifiers for exudate detection: Neural Networks with Multilayer Perceptron (MLP), Radial Basis Function (RBF) and Support Vector Machines (SVM). In 2012, Giancardo et al. [16] created a feature set based on wavelet decomposition and adaptive color vector representation for automatic and unsupervised exudate segmentation. In 2014, Zhang et al. [17] proposed a classification methodology using random forests based on geometric features extracted from the normalized images. In 2017, Fraz et al. [18] proposed an algorithm that combines morphological reconstructions, Gabor filter banks and a bootstrap decision tree for multiscale segmentation of exudates. To overcome the threshold selection issue for exudate detection, Kaur and Mittal [19] employed a dynamic thresholding method to detect exudate boundaries. Although they achieved good specificity and accuracy, sensitivity was only 0.88 (details reported in section 5).

Deep learning (DL) methods have an advantage of automatic feature extraction and they have achieved promising results in different computer vision and image analysis applications including automatic fundus image analysis [20–22]. In 2015, Prentašić and Loncaric [23] developed a ten-layered CNN to detect exudates. However, it had low sensitivity (0.77). Perdomo et al. [24] used a different CNN architecture and achieved a sensitivity of around 0.90 but the specificity was poor (0.40). While Yu et al. [25] and Prentašić et al. [26] achieved a reasonable sensitivity (0.88), their method required manual pre-processing steps for optic disk removal and vessel segmentation. Tan et al. [22]

* Corresponding author.
E-mail addresses: Parham.khojasteh@student.rmit.edu.au (P. Khojasteh), leandropassosjr@gmail.com (L.A. Passos Júnior), tiagojc@ifsp.edu.br (T. Carvalho), edmar.rezende@gmail.com (E. Rezende), behzad.aliahmad@rmit.edu.au (B. Aliahmad), papa@fc.unesp.br (J.P. Papa), dinesh@rmit.edu.au (D.K. Kumar).

https://doi.org/10.1016/j.compbiomed.2018.10.031
Received 25 July 2018; Received in revised form 27 October 2018; Accepted 27 October 2018

overcame the shortcomings of manual feature extraction and pre-processing, and their sensitivity was 0.87.

CNN-based methods do not require hand-crafted feature extraction but, it is necessary to identify suitable architectures and optimal parameters. As there is no exact method for selection of the network parameters such as the number of convolutional layers and filter sizes, these have been determined heuristically [27]. The size of the datasets is another limitation of using such networks because the full training of these requires large volumes of data. For overcoming these limitations, there is a need to investigate different deep learning methods and identify a network that gives good performance and is not reliant on large datasets.

The aim of this study was to identify a suitable deep learning method for good performance and to overcome the limitations mentioned above. We have compared the performance of multiple deep learning methods, and both, supervised and unsupervised classifiers. The CNN model, pre-trained residual networks (ResNet-50) with a supervised classifier and Discriminative Restricted Boltzmann Machines (DRBM) were investigated. The sensitivity, specificity and accuracy of the proposed methods were compared with previous works using two publicly available databases: (i) DIARETDB1 and (ii) e-Ophtha. The novelty of this work is that it has compared the performance of different deep learning methods for detection of exudates in the fundus images.

The remainder of this paper is organized as follows. Section 2 presents the theoretical background of the techniques used in this paper. Section 3 describes the experiments conducted to compare the different deep-learning methods adopted for exudate detection. The results are presented in section 4 and discussed in section 5 followed by conclusions and future works in section 6.

2. Theoretical background

This research has considered three deep learning techniques (i) CNN, (ii) pre-trained residual network with a classifier, and (iii) DRBM-based model. This section presents a brief description of these approaches.

2.1. Convolutional Neural Networks

The first few layers of the CNN have convolutional kernels and are for feature extraction, while the latter layers perform classification. Designing a suitable architecture requires selection of size and number of convolutional layers and the fully connected layers. We have used four convolutional layers for the feature extraction step, where each layer comprises 16 feature maps, each of size 3×3 pixels. A rectified linear unit was employed to avoid saturation of the neuron output. Max-pooling layers of size 2×2 with normalization were used after each convolutional layer for dimensionality reduction to enhance the convergence rate. 16 features from the last pooling layer were fed to a fully-connected layer with 100 neurons, the output of which was classified by a network of two neurons, each corresponding to one target class. The loss function used for training is presented in equation (1):

$$L = -\frac{1}{M}\sum_{i=1}^{M} \ln(p(x_i|y_i))) \tag{1}$$

where M stands for the size of training set, and $x_i \in \Re^n$ and $y_i \in \Re$ represent the i^{th} training sample and its corresponding label, respectively. Stochastic Gradient Descent (SGD) [28] was used to update network parameters as follows:

$$\theta^{t+1} = \theta^t - \eta\frac{\delta L}{\delta \theta} + \alpha\Delta\theta^t + \beta\eta\theta^t. \tag{2}$$

The network parameters, i.e., connection weights and biases, are θ, and θ^t is the updated θ at time step t. Parameters η, α, and β denote the learning rate, momentum, and weight decay, respectively. Fig. 1 shows the hierarchical architecture of the proposed network where I, C, FM, MP, NM, FC denote the input image, convolutional layer, feature map, max pooling, normalization layer, and fully-connected layer, respectively.

2.2. Deep residual networks

This uses a pre-trained model where the convolutional layers are pre-trained and do not require a large amount of data for training the network from scratch. Such an approach overcomes the limitations of using deep learning for medical images where the datasets are typically small. In this study, Residual Network (ResNet-50) [27] which was pre-trained using ImageNet dataset [29] has been used but the associated fully-connected softmax layer was replaced with supervised classifiers. Three classifiers were tested and have been described below.

The convolutional layers had filters of sizes 1×1, 3×3, and 1×1. The overall architecture followed two design rules: (i) for the same output size, the layers should have the same number of filters and (ii) if the feature map size is halved, the number of filters should be doubled. Max-pooling layers were performed directly by convolutional layers with the stride of 2 followed by batch normalization after each convolution operation and before ReLU [30] activation function.

The rules for the residual block shortcuts were based on the relative dimension of input and output. When the input and output had the same dimension, an identity shortcut was applied. When the difference in the dimension of the input and output increased, the shortcuts, there were two options: (i) extra zero entries were padded for increasing dimensions (notice that this option introduces no extra parameter), and (ii) the projection shortcut was used to match dimensions (performed by 1×1 convolutions). For both options, when the shortcuts go through the feature maps of two sizes, they are performed with a stride of 2.

The ResNet-50 model was pre-trained for the object detection task on the ImageNet 2012 dataset with 1.28 million images from 1,000 classes. We then used the first 49 layers of ResNet-50 as feature extractors to generate deeply-learnable features which were then fed to the classifier. The weights learned from the first step were kept the same, and we added an extra layer composed of different supervised classifiers which are described in the next section. Three different classifiers were considered: Support Vector Machine (SVM), Optimum-Path Forest (OPF), and k-Nearest Neighbors (KNN). These have been discussed below.

2.2.1. Support Vector Machines

SVM is a non-probabilistic, binary, linear classifier based on statistical learning theory. It uses kernels for transforming the feature space such that after transformation the samples from two different classes are linearly separable. It uses soft margins to maximize the inter-class distance.

2.2.2. Optimum-Path Forest

OPF [31–33] is a graph-based supervised approach whose training samples are represented as nodes in a graph, and the distance between them corresponds to the weight of the two nodes. The training step consists of finding the most representative samples (i.e., the prototypes) for each class, thus obtaining the optimal partition (according to some path-cost function) of the graph representing this training set. The classification of a test sample is achieved by computing its optimum-paths to the whole training graph and assigning to it the label of the root (i.e., prototype) whose path has strongest connections.

2.2.3. k-Nearest Neighbors

In the k-NN, data is classified based on the majority votes of its neighbors [34]. The object is assigned to the class that is most frequent in its k-sized neighborhood. In the simplest form, if $k = 1$, then the object is assigned to the class of its nearest neighbor. In this work, we have considered different values of k.

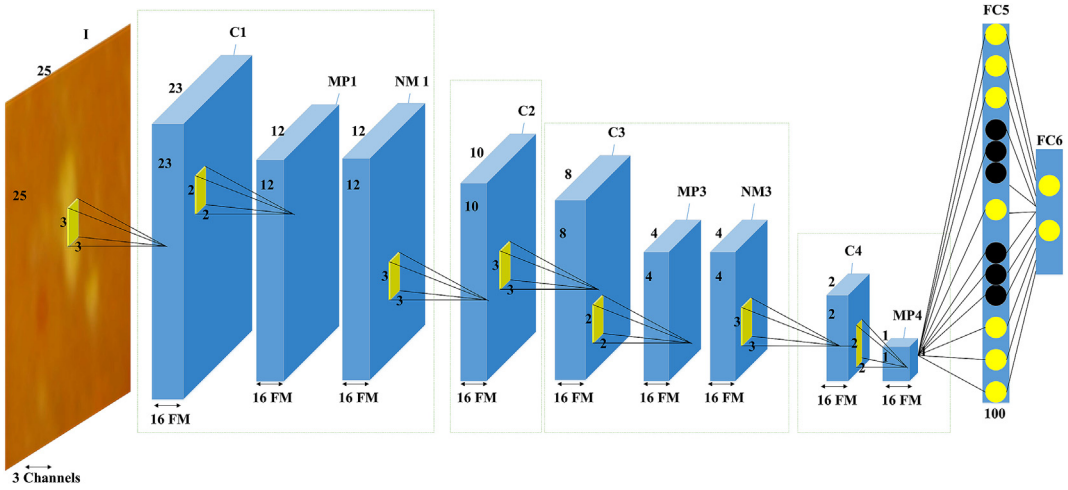

Fig. 1. Architecture of the proposed CNN used in this work.

2.3. Discriminative Restricted Boltzmann Machines

Restricted Boltzmann Machines (RBMs) is an unsupervised computational model approach [35] which can be interpreted as a bipartite graph. The input and hidden layers are connected to each other, and a training process updates the connection weights to minimize the reconstruction error between the input and the output data. Larochelle and Bengio [36] proposed a modified RBM which includes classification step and named it Discriminative Restricted Boltzmann Machine (DRBM). This comprises one additional input layer, i.e., the label layer, which contains the label of each input sample using one-hot encoding. This additional layer is connected to both, the hidden and visible layers, but with a different set of weights.

3. Material and methodology

In this section, we present the methodology adopted in the work, datasets, and the proposed approach.

3.1. Material

3.1.1. Dataset

In this work, two publicly available databases were used: (i) DIARETDB1 and (ii) e-Ophtha, whose details are given below.

DIARETDB1. This dataset comprises 89 fundus images of size 1500 × 1152 [37]. All images were taken by digital fundus camera with a 50° field of view. The annotation of exudates were manually performed and evaluated by four independent experts. Hard and soft exudates were considered as a single class called “exudate”.

e-Ophtha. E-Ophtha database was generated from a telemedical network developed for DR screening purpose [38]. This dataset provides 47 fundus images with manually annotated exudates. Because size of images image vary from 1400 × 960 to 2544 × 1696 pixels, all images were rescaled to the size of images in the DIARETDB1 database (1500 × 1152 pixels). The scale size was estimated based on the average size of the optic disk (OD). Fig. 2 shows sample images of the DIARETDB1 and e-Ophtha datasets from both, healthy individuals and patients with DR.

3.1.2. Data preparation

The size of the exudates vary, and thus the patch size required to box these can be very different. Fig. 3 shows a variation of patch sizes corresponding to all extracted patches, where the *X* and *Y* axes correspond to the length and width of a patch. It shows that after ignoring the outliers, the range of exudate patch varies from (25 × 25) to (286 × 487). To have one size of the patch for the analysis of the image, this was selected to be the smallest patch corresponding to the smallest pathological sign identified by the examiners. This is similar to the work reported by Shan and Li [39] and Cao et al. [40] on the same database (DIARETDB1).

In this study, we used patches of size 25 × 25 with three color channel (i.e. Red, Green, Blue (RGB)) which were labeled in two groups: (i) Exudate and (ii) Non-exudate. As a result, 67,600 and 23,200 exudate patches were manually extracted from the DIARETDB1 and e-Ophtha databases, respectively. To obtain a balanced dataset, 70,000 and 25,000 non-exudate patches were extracted from the regions without exudate from the two databases. Non-exudate patch group contained vessels, background tissues and optic nerve heads. All patches were extracted without any overlap. Figs. 4 and 5 illustrate patch samples from exudate and non-exudate classes used in this study.

3.2. Methodology

Fig. 6 shows the flowchart of the tasks. Pre-labeled exudate and non-exudate patches were used for training and testing the three deep-learning methods: (i) CNN, (ii) ResNet-50 + classifier (three different types), and (iii) DRBMs. In the ResNet-50, the softmax layer of the original architecture was replaced with three different classifiers: OPF, SVM, and *k*-NN. 10-fold cross-validation with ten runs technique was used to evaluate each method.

4. Network design

In this section, the network setup and corresponding results are presented.

4.1. Network setup

4.1.1. CNN model

The CNN parameters were obtained empirically as follows (discussed in section 5): learning rate = 0.01, momentum = 0.9, and the variance corresponding to the Gaussian filters for the convolutional layers was set to 0.01. Optimization was performed using stochastic gradient descent with the step-down policy and step size of 33. The batch sizes for training, validation, and test phases were 128, 32 and 32, respectively.

The CNN was implemented on Caffe platform [41] with a Geforce GTX 1070 graphics card. The optimum number of epochs was identified after evaluating the network during the training procedure for 40 epochs. Fig. 7 shows the convergence curve during training using the

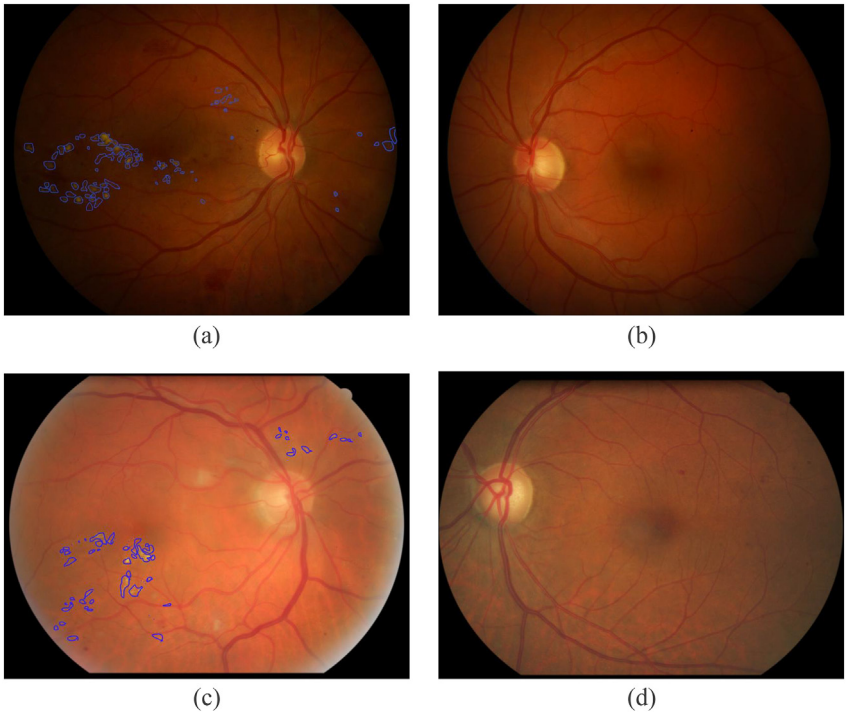

Fig. 2. Samples from DIARETDB1 and e-Ophtha databases where exudates are highlighted in blue: DIARETDB1 (a) patient and (b) control, and e-Ophtha (c) patient and (d) control.

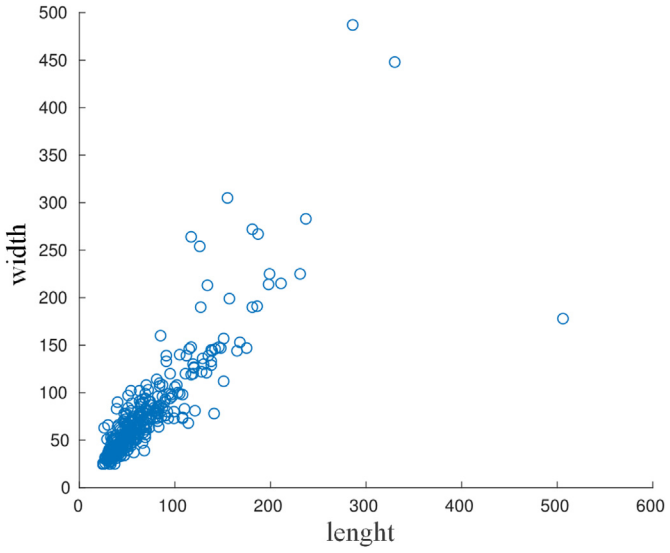

Fig. 3. Samples of exudate patches.

DIARETDB1 database.

From Fig. 7, it is observed that there was a significant improvement in the accuracy and reduction in loss after the 5^{th} epoch. The accuracy saturated around the 30^{th} epoch, where its value reached 90.6%. Thus the number of epochs was fixed to 30 for training and corresponding weights were used for the test phase.

4.1.2. Deep residual networks

The patches corresponding to exudate and non-exudate groups were resized to 224 × 224 to match the input image size required by Resnet-50. Feature reduction was applied to the 2048-dimensional output feature vector of the last convolution layer using Principal Component Analysis (PCA) [42] for dimensionality reduction and 100-dimensional features were obtained. Three classifiers were investigated in this study: OPF, SVM, and *k*-NN. The classifier parameters were optimized using a grid-search approach. The results obtained from each classifier were compared with the ones obtained by Resnet-50 with softmax layer.

4.1.3. DRBM

To apply an image to DRBM model, the intensity value of the pixels in the RGB space (i.e., pixels from each patch) were normalized to the range of [0,1]. The three channels of each patch were concatenated to one vector which was the input for the DRBM model.

Contrastive Divergence training algorithm using single sampling for each iteration was used and trained with mini-batches of size 100 and 200 epochs. The meta-parameters such as learning rate and the number of hidden units were optimized using a grid-search as shown in Fig. 8. It was observed that the higher accuracies (values in dark red) were located in the central region of the heat map and thus the number of hidden neurons was selected to be in the range [3,000 − 4,000], and learning rate in the range [0.1 − 0.17].

4.2. Results

The performance of the different methods was evaluated using the measures described by Loong [43]: overall accuracy (ACC), sensitivity (SN), and specificity (SP). The mean results obtained from 10-fold cross-validation approach with 10 runs corresponding to DIARETDB1 and e-Ophtha databases are presented in Table 1 and Table 2, respectively.

From Tables 1 and 2 it is seen that the performances for both the databases were similar. For DIARETDB1 database, “Resnet-50 + SVM” achieved the best sensitivity and accuracy of 0.99 and 98.2%, respectively. “Resnet-50 + OPF” obtained the highest specificity (0.99) compared to “Resnet-50 + SVM”, “Resnet-50 + KNN” and CNN model with the specificities of 0.96, 0.95 and 0.91, respectively. The “Resnet-50 + SVM” model also performed the best for e-Ophtha database. It is observed that the Residual Networks outperformed the CNN and DRBM models.

Since the best results were achieved through “Resnet-50 + SVM”,

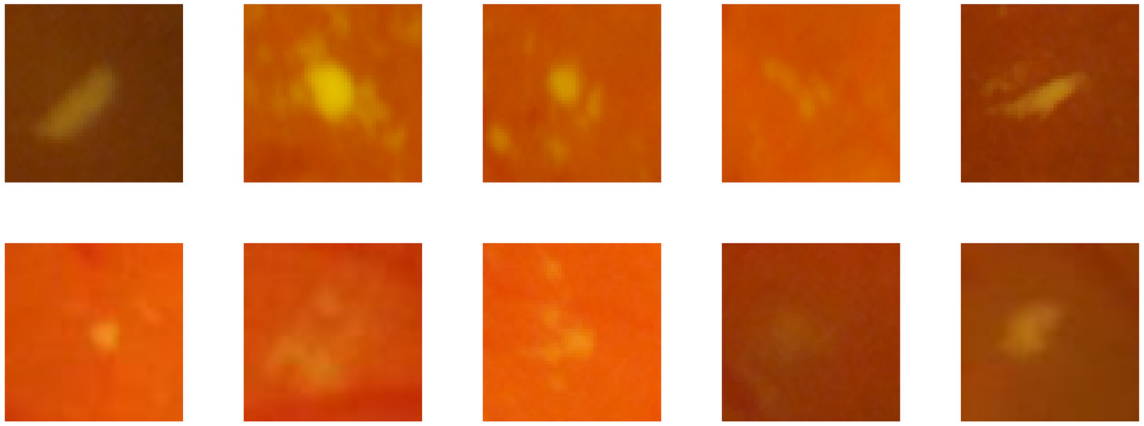

Fig. 4. Samples of exudate patches.

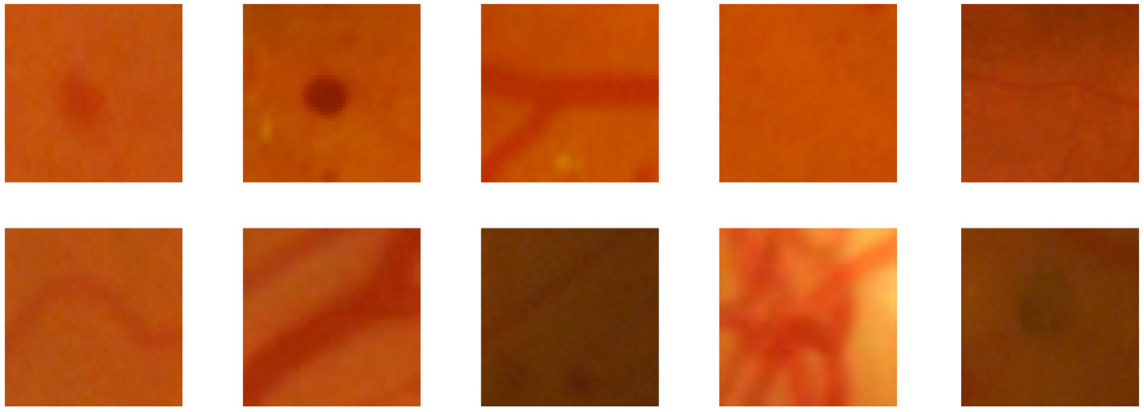

Fig. 5. Samples of non-exudate patches.

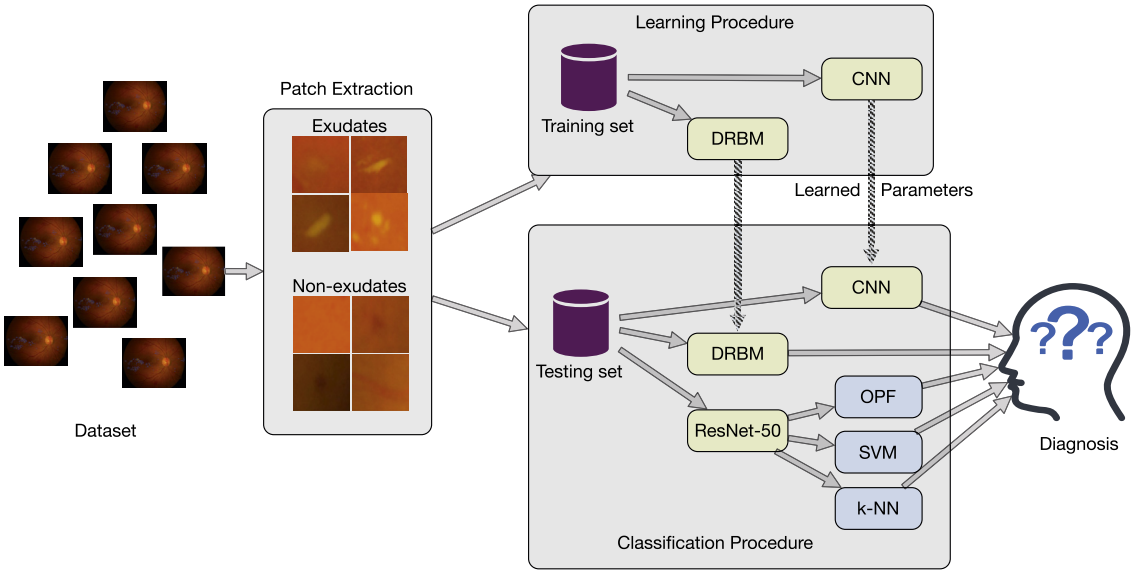

Fig. 6. Flowchart for detecting exudate and non-exudate patches.

this was used to compare with works reported in the literature (Table 3). For the DIARETDB1 database, the proposed approach (i.e., "Resnet-50 + SVM") achieved significantly better sensitivity compared to worked by Jaafar et al. [8] (0.99 vs 0.89), while both methods obtained similar accuracies. It also achieved significantly better accuracy (98.2%) and specificity values (0.96) compared with Fraz et al. [18]. For the e-Ophtha database, the proposed method outperformed the recent work by Mo et al. [44] with 0.18 improvement in sensitivity, but there was 0.04 decrease in the specificity.

5. Discussion

This study has investigated three deep learning techniques for the detection of exudates using fundus images. The results show that there

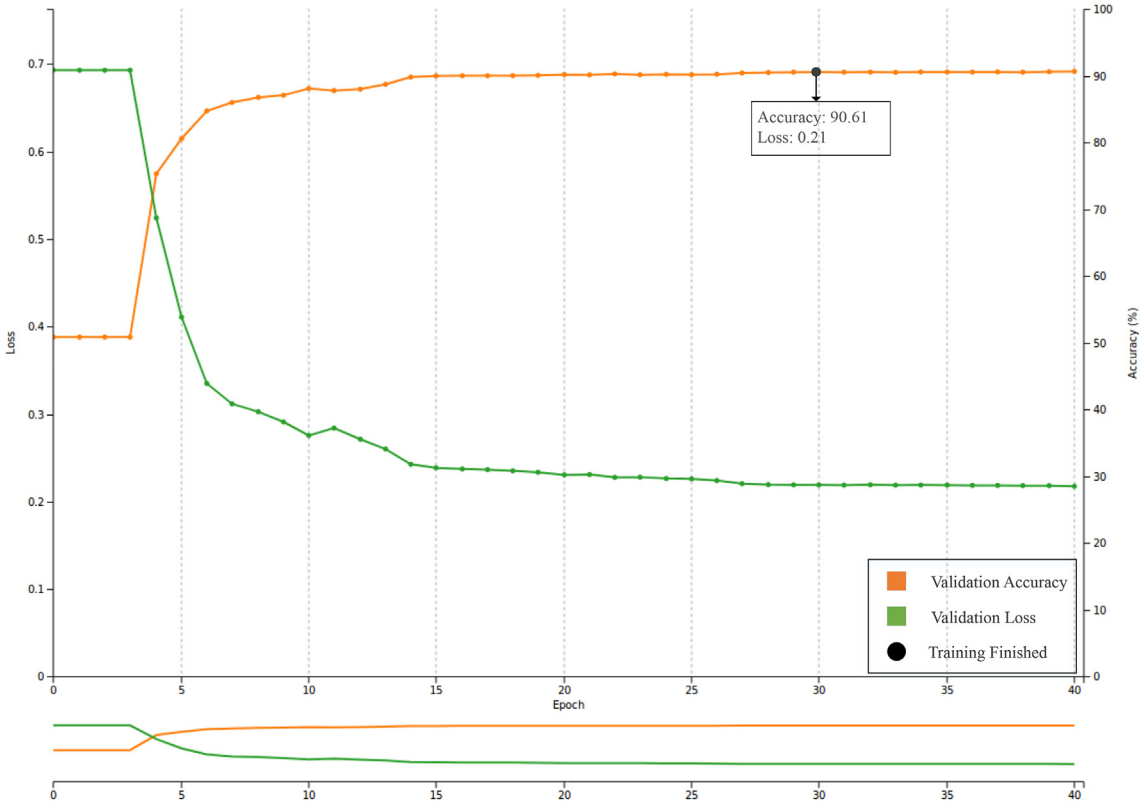

Fig. 7. Accuracy and loss changes over 40 training epochs concerning the DIARETDB1 database. A saturation is observed after the 30^{th} epoch.

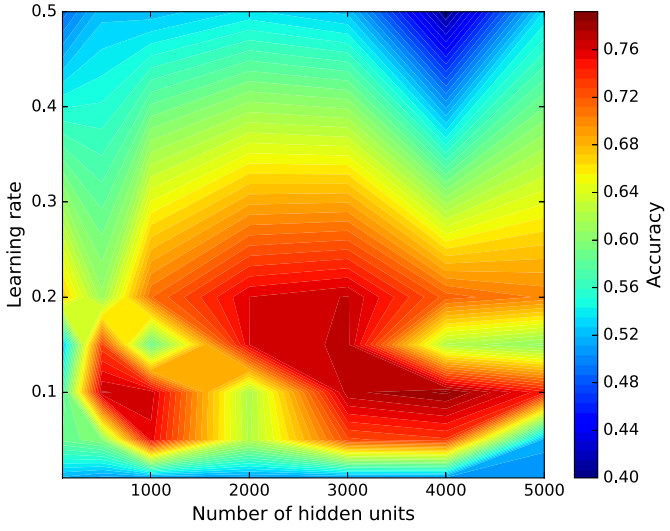

Fig. 8. Heat map obtained from the grid-search showing the best combination of learning rate and the number of hidden units.

Table 1
Performance of the proposed methods for DIARETDB1 database: overall accuracy, sensitivity, and specificity.

Technique	ACC	SN	SP
CNN	90.6%	0.90	0.91
ResNet-50 + KNN	97.1%	0.98	0.95
ResNet-50 + OPF	95.7%	0.93	0.99
ResNet-50 + SVM	98.2%	0.99	0.96
DRBM	76.37%	0.70	0.78

Table 2
Performance of the proposed methods for e-Ophtha database: overall accuracy, sensitivity, and specificity.

Technique	ACC	SN	SP
CNN	89.1%	0.89	0.91
ResNet-50 + KNN	96.0%	0.98	0.91
ResNet-50 + OPF	94.7%	0.90	0.99
ResNet-50 + SVM	97.6%	0.98	0.95
DRBM	70.37%	0.70	0.78

Table 3
Comparison of the proposed approach against other works reported in the literature. The symbol '-' stands for unreported results.

Database	Technique	ACC	SN	SP
DIARETDB1	**Proposed Method**	**98.2%**	**0.99**	**0.96**
	Fraz et al. [18]	87%	0.92	0.81
	Jaafar et al. [8]	99.0%	0.89	0.99
	Welfer et al. [45]	–	0.70	0.98
	Walter et al. [7]	–	0.76	–
	Harangi et al. [46]	82%	0.86	–
	Harangi et al. [10]	–	0.73	–
e-Ophtha	**Proposed Method**	**97.6%**	**0.98**	**0.95**
	Mo et al. [44]	–	0.92	–
	Das et al. [47]	–	0.85	–
	Imani et al. [48]	–	0.80	0.99
	Liu et al. [49]	–	0.76	–

is a significant difference in the results (i.e., accuracy, sensitivity, and specificity). The accuracy obtained using "Resnet-50 + SVM" (i.e. 98%) was the highest among all methods with sensitivity and specificity values as of 0.99 and 0.96, respectively. The performance achieved by "Resnet-50 + SVM" was significantly better than the other methods considered in this study, as well as those reported in the literature. However, there is potential for further improvements with

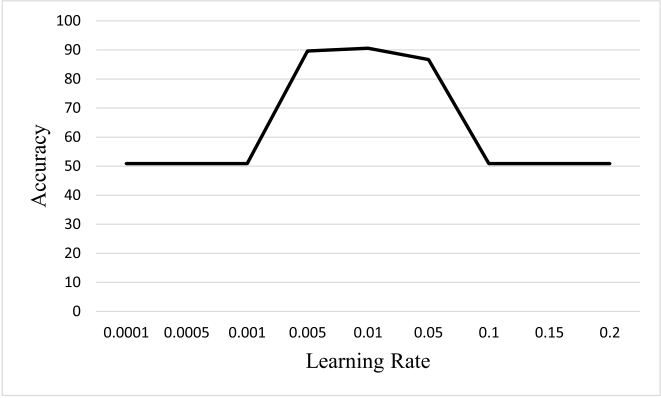

Fig. 9. Accuracy values over 40 training epochs considering the DIARETDB1 database. A saturation can be observed after the 30^{th} epoch.

computationally efficient classifiers, and the specificity may be improved using approaches such as Twin SVM.

The CNN-based model requires investigation on finding suitable parameters, which is one of the challenging tasks when using such models. earning rate is important for the network convergence and hence the effect of different learning rates, ranging from 0.0001 to 0.2, was investigated while momentum and variance were fixed to 0.01. Fig. 9 shows the accuracy of the network corresponding to different learning rates, where the best accuracy (90.6%) corresponded to learning rate of 0.01, which was similar to that reported in Alexnet experiments [50]. It was also found that learning rates less than 0.001 and larger than 0.1 resulted in the network not converging and were not evaluated further. Because the proposed CNN architecture was a modified version of the Alexnet, other parameters (i.e., batch size, momentum, and variance) were set as the same as of the Alexnet model.

The results show that DRBMs achieved an accuracy of only 73%. This poor performance can be attributed to a number of reasons such as preparation of data, and the shallow architecture. Normalized vectors used as the input of the DRBM were obtained by the concatenation of the three color channels (i.e., red, green, and blue) to obtain a single vector. This may not be the best method for representation of an image as an input of the DRBM. In this study, the DRBMs were used without additional layers such as used for Deep Belief Networks and Deep Boltzmann Machines. Thus, the tested network was comparatively shallow, while the deeper networks would be capable of extracting more detailed and intrinsic information from the data.

This work has shown that the selection of the parameters for CNN and DRBM models is challenging because there are no direct rules. Additionally, a limited number of samples for training purposes might have an impact on the performance of the network. One advantage of using "Resnet-50" is that it does not require a large training dataset.

Another point that deserves attention concerns the OPF classifier. Although it did not outperform SVM relating to the overall accuracy, it obtained the best specificity (i.e. 0.99). Additionally, OPF is parameterless and much faster for training should be explored in the future.

The results obtained in this paper show that pre-trained deep-learning methods have the potential for detecting exudates in retinal images. This can significantly help the experts to obtain better, faster and more accurate estimation of exudate spots on the retina. The choice of the network parameters has been found to be important for obtaining good results and our experiments suggest the use of "Resnet-50 + SVM".

6. Conclusions

The novelty of this work is that it has compared different deep-learning approaches for automatic detection of exudate based on the experimentally obtained accuracy, sensitivity, and specificity. It has shown that "Resnet-50 + SVM" is the best among these for automatic detection of exudates in the fundus images, especially the sensitivity, which is important for medical diagnostics. This method also has the advantage of incorporating pre-trained feature extraction layers which does not require large datasets for training.

This work has shown that the outcome of a deep-learning approach is dependent on the choice of the parameters. The next steps are to investigate other deep neural networks such as Generative Adversarial Networks. It is also important to determine the most appropriate method for presenting the data to the networks. Data augmentation through synthetic image generation and DBMs could be considered to build generative models that can better aggregate different color channels than their concatenation.

Conflicts of interest

The authors have no affiliations with or involvement in any organization or entity with any financial interest or non-financial interest in the subject matter or materials discussed in this manuscript.

Acknowledgments

The authors are grateful to FAPESP grants #2013/07375-0, #2014/12236-1, #2016/19403-6, and #2016/50022-9, as well as CNPq grant #307066/2017-7. This study was also financed in part by the Coordenação de Aperfeiçoamento de Pessoal de Nível Superior - Brasil (CAPES) - Finance Code 001.

References

[1] M.R.K. Mookiah, U.R. Acharya, C.K. Chua, C.M. Lim, E.Y.K. Ng, A. Laude, Computer-aided diagnosis of diabetic retinopathy: a review, Comput. Biol. Med. 43 (12) (2013) 2136–2155 https://doi.org/10.1016/j.compbiomed.2013.10.007 http://www.sciencedirect.com/science/article/pii/S0010482513002862.

[2] G. Leontidis, A new unified framework for the early detection of the progression to diabetic retinopathy from fundus images, Comput. Biol. Med. 90 (2017) 98–115 https://doi.org/10.1016/j.compbiomed.2017.09.008 http://www.sciencedirect.com/science/article/pii/S0010482517302986.

[3] N. Cheung, P. Mitchell, T.Y. Wong, Diabetic retinopathy, Lancet 376 (9735) (2010) 124–36, 1474-547x.

[4] Q. Mohamed, M.C. Gillies, T.Y. Wong, Management of diabetic retinopathy: a systematic review, Jama 298 (8) (2007) 902–916.

[5] J.E. Shaw, R.A. Sicree, P.Z. Zimmet, Global estimates of the prevalence of diabetes for 2010 and 2030, Diabetes Res. Clin. Pract. 87 (1) (2010) 4–14.

[6] W. Hsu, P.M.D.S. Pallawala, L. Mong Li, E. Kah-Guan Au, The role of domain knowledge in the detection of retinal hard exudates, Proceedings of the IEEE Computer Society Conference on Computer Vision and Pattern Recognition, vol. 2, 2001, pp. 246–251.

[7] T. Walter, J.C. Klein, P. Massin, A. Erginay, A contribution of image processing to the diagnosis of diabetic retinopathy-detection of exudates in color fundus images of the human retina, IEEE Trans. Med. Imag. 21 (10) (2002) 1236–1243.

[8] H.F. Jaafar, A.K. Nandi, W. Al-Nuaimy, Detection of exudates in retinal images using a pure splitting technique, Annual International Conference of the IEEE Engineering in Medicine and Biology, 2010, pp. 6745–6748.

[9] S. Ali, D. Sidibé, K.M. Adal, L. Giancardo, E. Chaum, T.P. Karnowski, F. Mériaudeau, Statistical atlas based exudate segmentation, Comput. Med. Imag. Graph. 37 (5–6) (2013) 358–368.

[10] B. Harangi, A. Hajdu, Detection of exudates in fundus images using a markovian segmentation model, 36th Annual International Conference of the IEEE Engineering in Medicine and Biology Society, 2014, pp. 130–133.

[11] C. Pereira, L. Gonçalves, M. Ferreira, Exudate segmentation in fundus images using an ant colony optimization approach, Inf. Sci. 296 (2015) 14–24.

[12] W.M.D.W. Zaki, M.A. Zulkifley, A. Hussain, W.H.W.A. Halim, N.B.A. Mustafa, L.S. Ting, Diabetic retinopathy assessment: towards an automated system, Biomed. Signal Process. Control 24 (2016) 72–82.

[13] A. Sopharak, B. Uyyanonvara, S. Barman, T.H. Williamson, Automatic detection of diabetic retinopathy exudates from non-dilated retinal images using mathematical morphology methods, Comput. Med. Imag. Graph. 32 (8) (2008) 720–727.

[14] C.I. Snchez, M. Garca, A. Mayo, M.I. Lpez, R. Hornero, Retinal image analysis based on mixture models to detect hard exudates, Med. Image Anal. 13 (4) (2009) 650–658.

[15] M. García, C.I. Sánchez, M.I. López, D. Abásolo, R. Hornero, Neural network based detection of hard exudates in retinal images, Comput. Methods Progr. Biomed. 93 (1) (2009) 9–19.

[16] L. Giancardo, F. Meriaudeau, T.P. Karnowski, Y. Li, S. Garg, K.W. Tobin Jr., E. Chaum, Exudate-based diabetic macular edema detection in fundus images using

publicly available datasets, Med. Image Anal. 16 (1) (2012) 216–226.
[17] X. Zhang, G. Thibault, E. Decencire, B. Marcotegui, B. La, R. Danno, G. Cazuguel, G. Quellec, M. Lamard, P. Massin, A. Chabouis, Z. Victor, A. Erginay, Exudate detection in color retinal images for mass screening of diabetic retinopathy, Med. Image Anal. 18 (7) (2014) 1026–1043.
[18] M.M. Fraz, W. Jahangir, S. Zahid, M.M. Hamayun, S.A. Barman, Multiscale segmentation of exudates in retinal images using contextual cues and ensemble classification, Biomed. Signal Process. Control 35 (2017) 50–62.
[19] J. Kaur, D. Mittal, A generalized method for the segmentation of exudates from pathological retinal fundus images, Biocybernetics and Biomedical Engineering 38 (1) (2018) 27–53.
[20] S.K. Saha, B. Fernando, D. Xiao, M.-L. Tay-Kearney, Y. Kanagasingam, Deep learning for automatic detection and classification of microaneurysms, hard and soft exudates, and hemorrhages for diabetic retinopathy diagnosis, Investig. Ophthalmol. Vis. Sci. 57 (12) (2016) 5962–5962.
[21] M.J.J.P. van Grinsven, F. Venhuizen, B. van Ginneken, C.C.B. Hoyng, T. Theelen, C.I. Sanchez, Automatic detection of hemorrhages on color fundus images using deep learning, Investig. Ophthalmol. Vis. Sci. 57 (12) (2016) 5966–5966.
[22] J.H. Tan, H. Fujita, S. Sivaprasad, S.V. Bhandary, A.K. Rao, K.C. Chua, U.R. Acharya, Automated segmentation of exudates, haemorrhages, microaneurysms using single convolutional neural network, Inf. Sci. 420 (2017) 66–76.
[23] P. Prentai, S. Lonari, Detection of exudates in fundus photographs using convolutional neural networks, 9th International Symposium on Image and Signal Processing and Analysis, ISPA, 2015, pp. 188–192.
[24] O. Perdomo, S. Otalora, F. Rodríguez, J. Arevalo, F.A. González, A novel machine learning model based on exudate localization to detect diabetic macular edema, Proceedings of the Ophthalmic Medical Image Analysis Third International Workshop, 2016, pp. 137–144.
[25] Y. Shuang Yu, Y. Di Xiao, Y. Kanagasingam, Exudate detection for diabetic retinopathy with convolutional neural networks, Conference Proceedings : … Annual International Conference of the IEEE Engineering in Medicine and Biology Society. IEEE Engineering in Medicine and Biology Society. Annual Conference 2017, 2017, p. 1744 http://ieeexplore.ieee.org/document/8037180/?reload=true.
[26] P. Prentašić, S. Lončarić, Detection of exudates in fundus photographs using deep neural networks and anatomical landmark detection fusion, Comput. Methods Progr. Biomed. 137 (2016) 281–292.
[27] K. He, X. Zhang, S. Ren, J. Sun, Deep residual learning for image recognition, IEEE CVPR, 2016, pp. 770–778.
[28] S. Pang, Z. Yu, M.A. Orgun, A novel end-to-end classifier using domain transferred deep convolutional neural networks for biomedical images, Comput. Methods Progr. Biomed. 140 (2017) 283–293.
[29] O. Russakovsky, J. Deng, H. Su, J. Krause, S. Satheesh, S. Ma, Z. Huang, A. Karpathy, A. Khosla, M. Bernstein, et al., Imagenet large scale visual recognition challenge, Springer IJCV 115 (3) (2015) 211–252.
[30] V. Nair, G.E. Hinton, Rectified linear units improve restricted Boltzmann machines, Proceedings of the 27th International Conference on Machine Learning (ICML-10), 2010, pp. 807–814.
[31] J.P. Papa, A.X. Falcão, C.T.N. Suzuki, Supervised pattern classification based on optimum-path forest, Int. J. Imag. Syst. Technol. 19 (2) (2009) 120–131.
[32] J.P. Papa, A.X. Falcão, V.H.C. Albuquerque, J.M.R.S. Tavares, Efficient supervised optimum-path forest classification for large datasets, Pattern Recogn. 45 (1) (2012) 512–520.
[33] J.P. Papa, S.E.N. Fernandes, A.X. Falcão, Optimum-path forest based on k-connectivity: theory and applications, Pattern Recogn. Lett. 87 (2017) 117–126.
[34] N.S. Altman, An introduction to kernel and nearest-neighbor nonparametric regression, Am. Statistician 46 (3) (1992) 175–185 http://www.jstor.org/stable/2685209.
[35] G.E. Hinton, Training products of experts by minimizing contrastive divergence, Neural Comput. 14 (8) (2002) 1771–1800.
[36] H. Larochelle, Y. Bengio, Classification using discriminative restricted Boltzmann machines, Proceedings of the 25th International Conference on Machine Learning, ACM, 2008, pp. 536–543.
[37] T. Kauppi, V. Kalesnykiene, J.-K. Kamarainen, L. Lensu, I. Sorri, A. Raninen, R. Voutilainen, H. Uusitalo, H. Kalviainen, J. Pietila, The diaretdb1 diabetic retinopathy database and evaluation protocol, Proceedings of the British Machine Vision Conference, BMVA Press, 2007, pp. 15.1–15.10, , https://doi.org/10.5244/C.21.15.
[38] E. Decencire, G. Cazuguel, X. Zhang, G. Thibault, J.C. Klein, F. Meyer, B. Marcotegui, G. Quellec, M. Lamard, R. Danno, D. Elie, P. Massin, Z. Viktor, A. Erginay, B. La, A. Chabouis, Teleophta: machine learning and image processing methods for teleophthalmology, IRBM 34 (2) (2013) 196–203 https://doi.org/10.1016/j.irbm.2013.01.010 http://www.sciencedirect.com/science/article/pii/S1959031813000237.
[39] J. Shan, L. Li, A deep learning method for microaneurysm detection in fundus images, 2016 IEEE First International Conference on Connected Health: Applications, Systems and Engineering Technologies, CHASE), 2016, pp. 357–358, , https://doi.org/10.1109/CHASE.2016.12.
[40] W. Cao, J. Shan, N. Czarnek, L. Li, Microaneurysm detection in fundus images using small image patches and machine learning methods, 2017 IEEE International Conference on Bioinformatics and Biomedicine (BIBM), 2017, pp. 325–331, , https://doi.org/10.1109/BIBM.2017.8217671.
[41] Y. Jia, E. Shelhamer, J. Donahue, S. Karayev, J. Long, R. Girshick, S. Guadarrama, T. Darrell, Caffe: Convolutional Architecture for Fast Feature Embedding, arXiv preprint. arXiv:1408.5093.
[42] J. Sarkar, S. Saha, S. Agrawal, An efficient use of principal component analysis in workload characterization-a study, AASRI Procedia 8 (2014) 68–74 2014 AASRI Conference on Sports Engineering and Computer Science (SECS 2014) https://doi.org/10.1016/j.aasri.2014.08.012 http://www.sciencedirect.com/science/article/pii/S2212671614000791.
[43] T.-W. Loong, Understanding sensitivity and specificity with the right side of the brain, BMJ 327 (7417). URL http://bmj.com/content/327/7417/716.full.pdf.
[44] J. Mo, L. Zhang, Y. Feng, Exudate-based diabetic macular edema recognition in retinal images using cascaded deep residual networks, Neurocomputing 290 (2018) 161–171 https://doi.org/10.1016/j.neucom.2018.02.035 http://www.sciencedirect.com/science/article/pii/S092523121830170X.
[45] D. Welfer, J. Scharcanski, D.R. Marinho, A coarse-to-fine strategy for automatically detecting exudates in color eye fundus images, Comput. Med. Imag. Graph. 34 (3) (2010) 228–235 https://doi.org/10.1016/j.compmedimag.2009.10.001 http://www.sciencedirect.com/science/article/pii/S0895611109001293.
[46] B. Harangi, A. Hajdu, Automatic exudate detection by fusing multiple active contours and regionwise classification, Comput. Biol. Med. 54 (2014) 156–171 https://doi.org/10.1016/j.compbiomed.2014.09.001 http://www.sciencedirect.com/science/article/pii/S0010482514002327Ωhttp://ac.els-cdn.com/S0010482514002327/1-s2.0-S0010482514002327-main.pdf?_tid=3947f220-681b-11e7-898b-00000aacb35e&acdnat=1499985359_0562d9956416c2c9d7ec76117d8d8082.
[47] V. Das, N.B. Puhan, Tsallis entropy and sparse reconstructive dictionary learning for exudate detection in diabetic retinopathy, J. Med. Imag. 4 (2) (2017) 024002.
[48] E. Imani, H.-R. Pourreza, A novel method for retinal exudate segmentation using signal separation algorithm, Comput. Methods Progr. Biomed. 133 (2016) 195–205 https://doi.org/10.1016/j.cmpb.2016.05.016 http://www.sciencedirect.com/science/article/pii/S0169260715301334.
[49] Q. Liu, B. Zou, J. Chen, W. Ke, K. Yue, Z. Chen, G. Zhao, A location-to-segmentation strategy for automatic exudate segmentation in colour retinal fundus images, Comput. Med. Imag. Graph. 55 (2017) 78–86 special Issue on Ophthalmic Medical Image Analysis https://doi.org/10.1016/j.compmedimag.2016.09.001 http://www.sciencedirect.com/science/article/pii/S0895611116300933.
[50] A. Krizhevsky, I. Sutskever, G. Hinton, Imagenet classification with deep convolutional neural networks, Commun. ACM 60 (6) (2017) 84–90.